Drape simulation of non-crimp fabrics

R.H.W. ten Thije, R. Loendersloot, R. Akkerman

University of Twente – P.O. Box 217, 7500 AE Enschede, the Netherlands
URL: www.composites.ctw.utwente.nl e-mail: r.h.w.tenthije@utwente.nl;

ABSTRACT: The draping process of non-crimp fabrics (NCF) on a doubly curved mould determines the fibre distribution and hence the processing and performance of the NCF product. A composite Finite Element (FE) model is developed to simulate the draping process of NCFs on arbitrary geometries. Tool-part interaction is taken into account. Problem regions with possible fibre buckling can be indicated and the fibre distribution in the final NCF is predicted. The model contains a novel modelling approach to simulate the slip of the individual fibre layers. Additional layers and degrees of freedom were added to a membrane element to simulate the slipping layers with one element through the thickness. This enables efficient FE simulations of the draping process. Several experiments were performed: measurement of the thickness change during shear deformation, fibre pull-out experiments and a drape experiment. The latter is compared with FE simulations.

Key words: NCF, non-crimp fabric, draping, finite element simulation

1 INTRODUCTION

Resin infused composite products based on non-crimp fabrics (NCF) can offer a cost effective alternative for prepreg technology. These stitch-bonded fabrics can be draped like woven fabrics, but do not show a significant drop in mechanical performance due to the absence of fibre undulation. This makes them applicable for use in aerospace and automotive parts that demand a high mechanical performance. The process of draping the NCF on the mould plays a key role for components that exhibit double curvature. The fibre distribution after draping dominates both the filling process and the mechanical performance of the finished part. An optimal design can be found by simulating both processing and performance. Numerical tools can also reduce the production of costly prototypes.
A Finite Element (FE) model was developed to simulate the draping process of NCFs on arbitrary geometries. The model identifies problem areas during the draping and it determines the fibre distribution in the final product.
This research focuses on non-crimp fabrics with a chain knit pattern. The resulting model can be adapted for non-crimp fabrics with different knit patterns by adjusting the stitch and shear behaviour. Four main deformation mechanisms can be identified in the chain knitted non-crimp fabric [1,2]:

1. Extension and compaction of the stitch material
2. In plane compaction of the fibres (during shear)
3. Rotation of the fibres (during shear)
4. Sliding of the fibres

These deformation mechanisms are described in a continuum formulation, based on semi-empirical laws. The continuum formulation of the mechanisms 1 to 3 and corresponding experiments to obtain the material properties were reported in [1]. The next section describes how the slip mechanism is implemented in the FE model.

2 MODELLING OF THE TOW SLIP

The possibility of the individual yarns to slide through the stitches is an unconventional part of the deformation, when comparing with the more common woven fabrics. Woven fabrics can show a small amount of slip, but the effect is neglected in most drape simulations. Fibre slip is not negligible for non-crimp fabrics. Draping a non-crimp fabric on a doubly curved shape immediately shows the large influence of the mobility of the yarns.

2.1 Continuum mechanics

Figure 1 shows a yarn that is slipping through the stitches in its own longitudinal direction *a.*

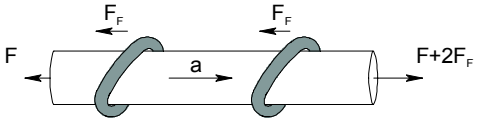

Fig. 1. Slip of the fibres relative to the stitches.

Movement in the other two dimensions is restricted by either the other yarns or the stitches. Each stitch

is interpreted as an obstacle that introduces friction. The increase in force F_F after passing a stitch is proportional to the slip velocity, based on a simplified viscous friction law. The traction τ on the layer interface is stated as: $\sigma \cdot n$, with σ the stress tensor and n the normal on the interface. Equilibrium between traction and internal stresses results into:

$$v_{sl} = \frac{1}{\eta}\frac{\partial \sigma_f}{\partial a} \tag{1}$$

with v_{sl} the slip velocity: the relative velocity of the fibres with respect to the stitches. The viscous slip coefficient η is a material parameter that depends on stitch tension and stitch density. σ_f is the fibre stress. The movement of the stitches is controlled by the continuum that captures the stitch deformation mechanism. The slip velocity can be expressed as the difference between the velocity of the fibres and the velocity of the continuum:

$$v_{sl} = v_f - v_c \tag{2}$$

with v_f the velocity of the fibres and v_c the velocity of the continuum. The strain rate of the fibres equals the fibre velocity gradient in the fibre direction and can be expressed using the velocity of the continuum and the slip velocity through equation (2).

$$\frac{\partial \varepsilon_f}{\partial t} = \frac{\partial v_f}{\partial a} = \frac{\partial v_{sl}}{\partial a} + \frac{\partial v_c}{\partial a} \tag{3}$$

The fibres are assumed to behave linearly elastic according to Hooke's law: $\sigma_f = E_f \cdot \varepsilon_f$, with σ_f the fibre stress, E_f the Young's modulus of the fibres and ε_f the strain in the fibres. For the fibre strain rate this results in:

$$\frac{\partial \varepsilon_f}{\partial t} = \frac{1}{E_f}\frac{\partial \sigma_f}{\partial t} \tag{4}$$

Combining equation (1), (3) and (4) leads to the following fibre slip equation:

$$\frac{1}{E_f}\frac{\partial \sigma_f}{\partial t} = \frac{1}{\eta}\frac{\partial^2 \sigma_f}{\partial a^2} + \frac{\partial v_c}{\partial a} \tag{5}$$

Equation (5) must hold for each fibre layer that is added to the continuum.

2.2 Finite element modelling

The deformation mechanisms 1 to 3 (*section 2*) were implemented with the use of constitutive laws. Continuum elements with nodal displacements as degrees of freedom are a common way to implement these constitutive laws. The equation that governs the slip mechanism, equation (5), obstructs a straightforward implementation of the complete material model into a FE formulation by the use of constitutive laws only. Multilayer elements were implemented to incorporate the fibre slip (*deformation mechanism 4*). An additional layer and an additional degree of freedom were added for each fibre layer. The additional nodal degree of freedom is the stress in the fibres σ^i_f. By having displacements and fibre stresses in one element, equation (5) can be solved for each fibre layer. Figure 2 shows an example of a two-layer element.

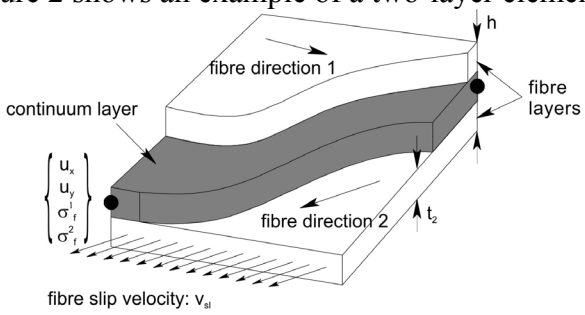

Fig. 2. Element with 2 fibre layers

Mechanical equilibrium for the complete element will result in the additional equation necessary to solve the complete system. Equilibrium for the total element results into:

$$\vec{\nabla}\left(\sigma_c + \sum_{i=1}^{n}\frac{t_i}{h}\sigma^i_f\right) = 0 \tag{6}$$

with σ_c the stress in the continuum layer, t the layer thickness, h is the total thickness, i denotes the layer number and n is the total number of fibre layers.

3 MATERIAL EXPERIMENTS

The experimental work was performed on a carbon biaxial NCF (± 45°), type 2A from Devold AMT with an aerial weight of 541 gr/m^2.

3.1 Fabric thickness

The assumption of a constant volume during shear deformation is often used in numerical calculations on fabrics. Trellis frame experiments were performed with a continuous thickness measurement to validate this assumption. The measuring device uses a Linear Variable Differential Transformer (LVDT) to measure displacements (*see figure 3*). The small spring exerts a pressure of ±0.5 kPa on the fabric. The thin rod is pushed through the fabric. The inner diameters of the surfaces that touch the fabric are 10 mm to keep clear of the local distortion created by the rod penetration. Three specimens were sheared and unsheared during three cycles.

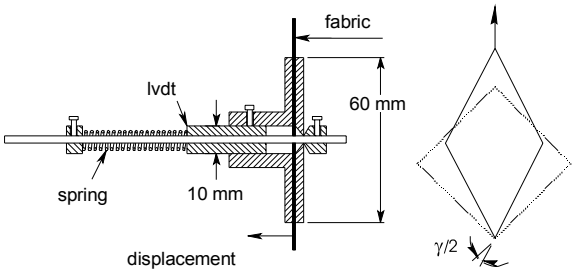

Fig. 3. (a) Fabric thickness measuring device and (b) definition of the shear angle.

Figure 4 shows the resulting fabric thickness for the first cycle from the start of the experiment up to a shear angle of 60° and a fit assuming a constant volume. Only the first cycle of the three was used, because that is when deformation takes place during the forming of NCF products.

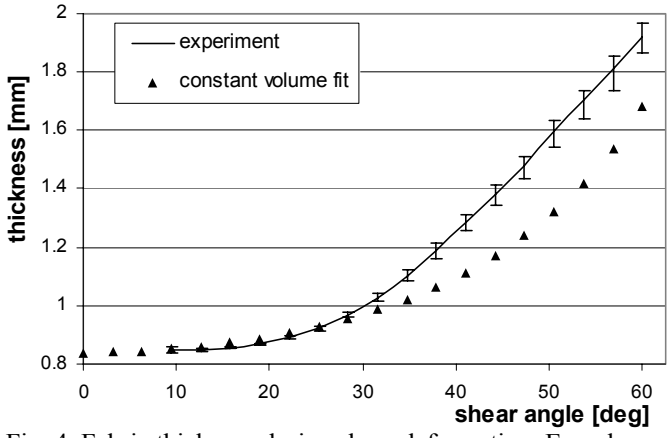

Fig. 4. Fabric thickness during shear deformation. Error bars indicate the maximum and minimum value found.

An initial shear angle of 8° was already present in the fabric. This could be due to a production error or was induced by the handling of the fabric. The forces needed to shear the fabric are very small [1] and unrolling and cutting the fabric can easily cause shear angles of a few degrees. The constant volume fit holds for shear angles below 30°, but at higher shear angles a dilatation phenomenon is observed. The thickness increases faster than expected based on a constant volume assumption, because the close packing of the fibres is disturbed. More detailed information about the setup, pictures and the results of the second and third cycle can be found in [3].

3.2 Fibre slip

Fibre pull-out experiments similar to those of Kong *et al*. [2] were performed to obtain the fibre slip parameters for the simulation. Figure 5 shows the results of these experiments. The force is given per square mm of contact area between the fibre layers. It is assumed that the traction between the layers is equally distributed over this area. Kong et al. used a much smaller pull-out width, but here the larger width is chosen to minimise the influence of the edge effects observed at the interface between slipping and non-slipping fibres. Fibres adjacent to the slipping fibres are partially pulled out and wrinkle. This increases the pull-out force. Experiments with smaller pull-out widths indicated that the edge effects are in an acceptable range of 5 to 10% for the 10 mm pull-out width. The results indicate that the friction between the layers is mainly of a Coulomb type below a pull-out length of 8 mm. The friction force steadily increases between 8 and 50 mm and a velocity dependent part is observed. Above 50 mm the friction force levels.

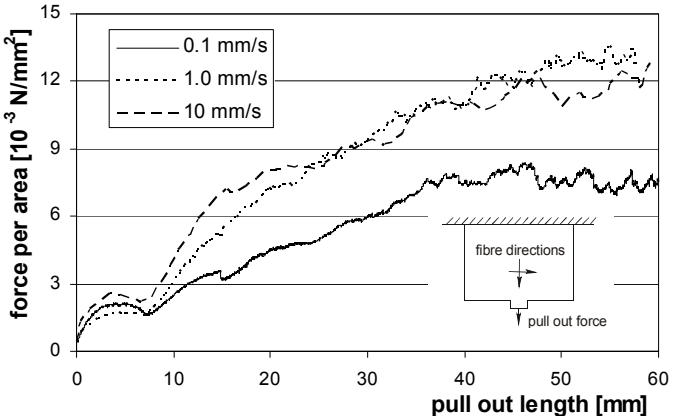

Fig. 5. Fibre pull-out forces at different velocities. wxh: 120mm x 80mm. pull-out width: 10mm.

4 DRAPE EXPERIMENTS AND SIMULATIONS

Drape experiments and corresponding simulations were performed on a topped cone geometry. Figure 6 shows the dimensions of the geometry, the setup of the simulation and the experimental setup.

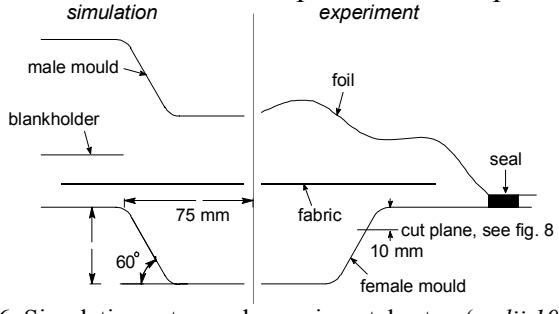

Fig. 6. Simulation setup and experimental setup (*radii 10mm*).

The experimental product was fabricated with the Resin Injection under Flexible Tooling (RIFT) process. The simulation uses two moulds. The blankholder is modelled to simulate the effect of the vacuum that presses the fabric on to the mould. Simulations without a blankholder showed severe wrinkling in the fabric, which is also observed in experiments if the fabric is shaped with two hard

moulds. Shaping under vacuum results in a more controllable way to perform the experiment.

The assumption of a constant volume is used, because the shear angles do not exceed 35° to 40° in practice. Although the experiments revealed that the friction between the fibre layers is mainly of a Coulomb type, the simulation was run with the viscous friction approach. Simulations show spatial instabilities depending on mesh size, material parameters and time step size. These instabilities were successfully eliminated for the viscous friction model, but not (yet) for the Coulomb type of friction. The moulds were closed with a speed of 20 mm/s during the simulation and the viscous traction was set to $1.45 \cdot 10^{-3}$ Ns/mm^4. A first simulation was done without tool-part friction and without a blankholder; a second one was done with a Coulomb type of friction between the part and the tool (*friction coefficient 0.2 [-]*) and a blankholder pressure of 0.15 bar. Figure 7 shows the final part shape and the resulting fibre stresses at the end of the second simulation.

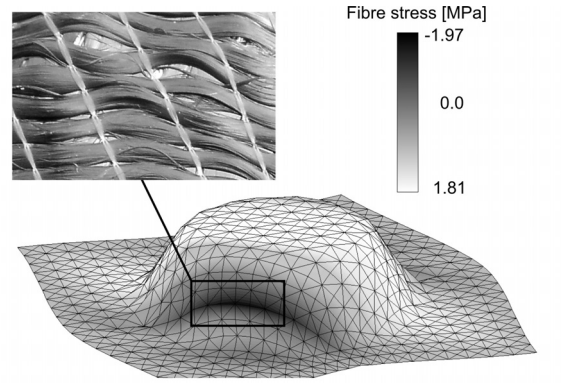

Fig. 7. Compressive fibre stresses predicted by the simulation and experimentally observed fibre buckling.

The regions with the highest compressive stresses correspond with the regions in the product where fibres start to buckle. Figure 8 shows the enclosed fibre angle between the two fibre layers at a circular cross section on the cutting plane shown in figure 6. The results were obtained by taking pictures perpendicular to the surface at the inner and outer surface at an interval of 15° along the circular cross section. The pictures were analysed manually.

The results of simulation 2 are symmetrical due to the blankholder and the friction. The fabric remains in the middle of the mould. Simulation 1 and the experiment show non-symmetric results mainly due to shifting and rotation of the fabric. The fabric is pulled into the mould from one side and not from all sides. This is very hard to control, which makes it difficult to compare simulations and experiments. The experimental procedure requires re-designing to obtain more reproducible results.

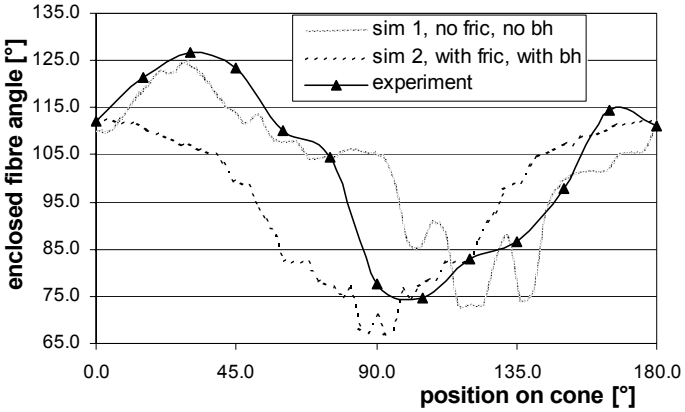

Fig. 8. Enclosed fibre angle in the cone drape experiment and two different FE simulations.

5 CONCLUSIONS AND FUTURE WORK

A composite finite element model that simulates the draping of a non-crimp fabric on arbitrary geometries was developed and implemented. The model simulates the slip of the individual fibre layers with the use of a viscous friction model and one element through the thickness. Preliminary experimental results show that the model is capable of predicting the final fibre orientation with an accuracy of 10 to 15° and identifies the regions that are susceptible to wrinkling due to compressive fibres stresses. More drape experiments and corresponding simulations will be performed to validate the model.

ACKNOWLEDGEMENTS

This work was performed with the support from the European Commission, by means of the FALCOM project (GRD1-2001-40184). This support is gratefully acknowledged by the authors.

REFERENCES

1. R.H.W. ten Thije, R. Loendersloot and R. Akkerman, Material characterisation for finite element simulation of draping with non-crimp fabrics, *Proceedings on the 6th International ESAFORM Conference on Material Forming*, Nuova Ipsa Editore, Palermo (2003), 859-862.
2. H. Kong, A.P. Mouritz and R. Paton, Tensile extension properties and deformation mechanisms of multiaxial non-crimp fabrics, *Composite Structures 66* (2004) 249–259.
3. S.V. Lomov, M. Barburski, Tz. Stoilova, I. Verpoest, R.Akkerman, R.Loendersloot, R.H.W.ten Thije, Carbon composites based on multiaxial multiply stitched preforms. Part 5: Biaxial tension, picture frame and compression tests of the performs, In Press*: Composites Part A.*